Appl. Phys. B 60, 135–143 (1995)

Applied Physics B Lasers and Optics

Three-dimensional spatial diffusion in optical molasses

T. W. Hodapp[1,*], C. Gerz[1,], C. Furtlehner[1,***], C.I. Westbrook[1,†], W.D. Phillips[1], J. Dalibard[2]**

[1] National Institute of Standards and Technology, U.S. Department of Commerce, Technology Administration, PHYS A167, Gaithersburg, MD 20899, USA (Fax: +1 301/975-3038)

[2] Laboratoire Kastler Brossel, Departement de Physique de l'Ecole Normale Supérieure, 24, rue Lhomond, F-75005 Paris, France (Fax: +33-1/45350076, E-mail: DALIBARD@physique.ens.fr.)

Received: 22 July 1994 / Accepted: 10 October 1994

Abstract. We have studied the expansion of a small cloud of ^{85}Rb atoms in three-dimensional optical molasses (lin $\perp$ lin and $\sigma^+ - \sigma^-$ configurations) and observed diffusive motion. We determined the spatial-diffusion coefficients for various laser intensities and detunings, and compared them (in the case of lin $\perp$ lin molasses) to values calculated from friction and momentum-diffusion coefficients of a one-dimensional (1D) theory of laser cooling. The predicted variations of the spatial-diffusion coefficient with laser intensity and detuning are in good qualitative agreement with the experimental data. We found that the minimal value observed experimentally, $\approx 6 \times 10^{-4}\,\mathrm{cm^2/s}$, lies within a factor of 3 of the 1D theoretical minimum, $\approx 26\hbar/M$, where M is the atomic mass.

PACS: 32.80.Pj; 42.50.Vk; 35.80.+s

Optical molasses is a configuration of laser beams which cools and viscously confines a gas of atoms. Viscous confinement refers to the fact that atoms in the molasses experience such a strong damping of their motion that their mean free path is much smaller than the dimensions of the molasses. The motion of the atoms is diffusive and confinement results from the fact that the time to diffuse out of the molasses region can be quite long.

The first theoretical treatments of optical molasses [1, 2] were in the context of 'Doppler cooling', i.e., a model in which atoms are treated as two-level systems interacting with low-intensity laser beams. Under these circumstances, one can calculate a spatial-diffusion coefficient D_x, and a time scale τ for atoms to escape from the molasses due to spatial diffusion. For example, according to the theory of Doppler cooling ([1] and Sect. 2E of [3]), the minimum diffusion coefficient for Rb atoms, laser cooled on the 780 nm resonance line, is $3 \times 10^{-2}\,\mathrm{cm^2/s}$, which corresponds to a molasses decay time of 800 ms for a sample radius of 5 mm. Initial measurements of the decay [1, 3] were in agreement with the early calculations and led to the feeling that the situation was well understood.

More recently, it was discovered [4] that the temperature of atoms in optical molasses was much lower than that predicted by Doppler-cooling theory. This led to a new theory of multi-level-atom laser cooling [5, 6] that explained the low temperatures, and predicted details of the dependence of temperature on laser intensity and detuning that were subsequently confirmed experimentally [7]. The new theory predicted [5] that the damping of atomic motion was much stronger than in the case of Doppler cooling. This implied not only much lower temperatures for the atoms, but also much reduced spatial diffusion. Molasses decay times expected on the basis of the damping and heating rates of [5] were often in excess of 100 s for a 1 cm diameter molasses. Such long times have never been observed.

In this paper, we present a detailed experimental and theoretical investigation of spatial diffusion. In Sect. 1, we introduce a method to directly measure the diffusion constant by observing the expansion of a cloud of atoms. This technique is more accurate and reliable than using the molasses lifetime to infer D_x. We find diffusion constants much lower than those measured previously. In Sect. 2, we re-examine the theory of spatial diffusion in optical molasses, taking into account some of the recent insights into the laser cooling process. These include the fact that the damping force may not be linear in velocity, that the distribution of atomic velocities may not be Maxwellian, and that the atom motion may be affected by the periodic array of potentials created by interfering laser beams. We find that these theoretical estimates are in reasonable agreement with our new measurements.

Dedicated to H. Walther on the occasion of his 60th birthday

* *Permanent address*: Hamline University, Physics Department, St. Paul, MN 55104, USA (Fax: +1-612/641-2956, E-mail: THODAPP@piper.hamline.edu)

** *Permanent address*: GAO Company, Euckenstrasse 12, D-81369 München, Germany (Fax: +49-89/76994-637)

*** *Current address*: Department of Physics, Ecole Normale Supérieure, 45, rue d'Ulm, F-75005 Paris, France

† *Permanent address*: Institut d'Optique Théorique et Apliquée, B.P. 147, Centre Universitaire d'Orsay, F-91403 Orsay Cedex, France (Fax: +33-1/69413192, E-mail: CHRISTOPH.WESTBROOK@iota.u-psud.fr)

1 Experiment

Our technique to measure D_x is to record images of a cloud of atoms, released from a Magneto-Optical Trap (MOT) [8], expanding in molasses. We use a CCD camera and a VCR to record a sequence of images (a movie). These images then are analyzed using a frame grabber to digitize the images. The size of the cloud as a function of time gives a measure of D_x. This technique is insensitive to any small overall drift velocity due either to imbalance of the beams or, in the $\sigma^+ - \sigma^-$ configuration, due to residual magnetic fields. If the drift is very large or if the expansion is non-isotropic, it is easily recognized and can be corrected. The method is also insensitive to losses due to background collisions or any other uniform loss, since we measure only the *shape* of the expanding cloud.

1.1 Realization of optical molasses

Our apparatus has already been described in [9]. Briefly, an atomic beam of neutral Rb was slowed by a pair of frequency-chirped diode lasers [10]. The slowed atoms entered a UHV region ($\approx 10^{-7}$ Pa) where a MOT captured them and confined them to a volume smaller than 1 mm^3. The laser beams for the MOT and molasses were derived from a Ti-Sapphire ring laser which was locked to a Rb saturated-absorption cell. Acousto-Optic Modulators (AOMs) permitted computer control of the offset frequency between the MOT or molasses laser beams and the locked frequency. Light from the Ti-Sapphire laser was then split off into three beams (one for each Cartesian axis) and passed through a liquid-crystal variable-retardation plate to allow computer selection of either circularly or linearly polarized beams. Each of the three beams were individually expanded with telescopes before entering the vacuum chamber. Care was taken in the optical setup to preserve the polarization of the light through all reflections. As each beam left the chamber, it passed through a quarter-wave retarder and was retro-reflected back through the quarter-wave plate and into the chamber. In this way, each axis had perpendicular, counter-propagating, linearly polarized beams (lin $\perp$ lin) when used with incoming linear-polarized light, or opposite-helicity, counter propagating, circular-polarized light (σ^+-σ^-) when circular light was brought into the chamber. The three beams were reduced in size by an aperture to an 18 mm diameter region over which the intensity varied less than 5%. The intensity was varied by manually rotating a half-wave plate in front of a linear polarizer. We did not vary the intensity electronically using the AOMs because of resulting changes in alignment caused by thermal effects in the AOM. A diode laser, frequency-locked to a saturated-absorption signal, was tuned to the F=2 ground state, and brought into the chamber along one of the MOT/molasses axis to repump atoms which fell into that ground state.

The magnetic field for the MOT was provided by a pair of water-cooled coils inside the vacuum system. Additional coils to cancel any residual magnetic fields were added outside. The residual field was nulled by minimizing the temperature of the molasses with respect to variations of the magnetic field [3]. The temperature was measured with a time-of-flight method. In this method the molasses lasers were switched off and the atoms dropped ballistically through a distance of approximately 5 cm after which they intersected a probe beam. The fluorescence induced by this beam was recorded and the time-of-flight signal yielded a temperature. Details of this technique are given in [4, 7, 9]. We estimate that the field present in the molasses region was less than 10μT.

1.2 Data acquisition

Each measurement began by switching on the MOT coils (and switching the MOT/molasses beams to circular polarization). In this way, a very small (< 1 mm) dense ($\approx 10^{10}$ atoms/cm^3) cloud of atoms formed near the center of the intersection of the molasses beams. After collecting atoms for about 2 s, the MOT was released by switching off the coils (in about 100 μs) and the polarization was returned to linear (in the case of lin $\perp$ lin measurements). After the coils were turned off, the frequency was changed (via the AOM) to the detuning to be used for the measurement. This change in frequency also affected the intensity, as the efficiency of the AOM was frequency dependent. The expanding cloud of atoms was recorded in a video-movie by a high-sensitivity CCD camera together with an on-screen clock to provide timing information. The first frames used in the data presented below began more than 100 ms after the detuning was changed to its final value. This allowed ample time for the velocity distribution of the cloud of atoms to reach the steady state.

Measurements were made for both lin $\perp$ lin and $\sigma^+ - \sigma^-$ molasses. Detunings in the lin $\perp$ lin case were varied from approximately 1 to 10 natural linewidths Γ on the low-energy (red) side of the resonance, and intensities ranged from about 0.5 to 3 mW/cm^2. The natural linewidth $\Gamma/2\pi = 5.89$ MHz for rubidium. The majority of the data were taken under lin $\perp$ lin conditions. Data for $\sigma^+ - \sigma^-$ polarizations were taken with detunings ranging from about 2 to 10 Γ.

1.3 Data analysis

Each of the movies was analyzed in the following way. A frame grabber was programmed to sample images at 100 ms intervals (every 3 frames) over the length of each movie. Each frame was then smoothed by replacing each pixel value (an 8-bit digitized intensity associated with each pixel) with an unweighted average of the surrounding 3×3 grid of pixels. Each pixel collected light from an area of about 5×10^{-3} mm^2 at the molasses. This technique provided better signal to noise for low-intensity frames without sacrificing accuracy. For each movie, the background level was found by locating and averaging over pixel regions where no atoms were present. For about 65% of the movies, the background was flat to ± 1 pixel value, however, for the remaining 35% of the data the background level was not uniform throughout the image. This variation in the background level was due to reflections of laser light scattered inside the vacuum chamber. Since it was not possible to unambiguously determine

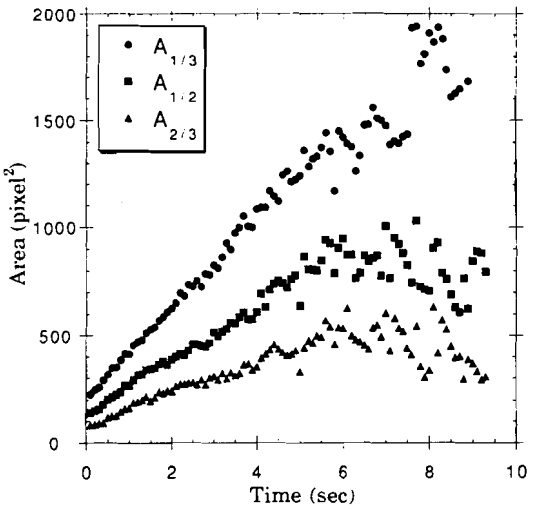

Fig. 1. Data from one movie. The increase in area is linear until the atomic cloud begins to reach the edge of the molasses after about 6 s. The three sets of data indicate the area A_β in number of pixels, in which the molasses intensity exceeded 1/3, 1/2, or 2/3 (β) of the peak intensity

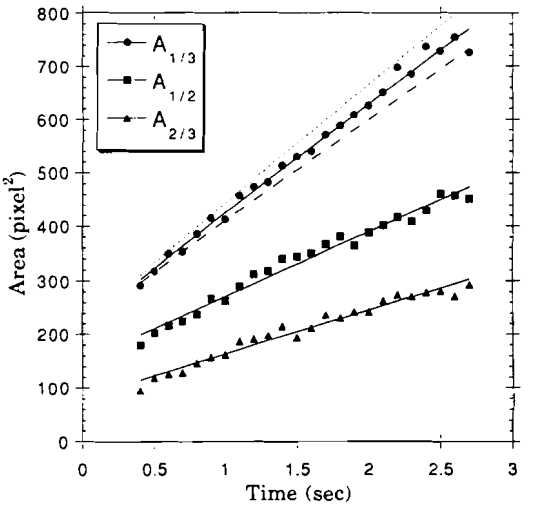

Fig. 2. The first few seconds of data from Fig. 1. Linear behavior here is indicative of diffusive motion. The *solid lines* indicate linear least-squares fits of the data. A measure of the self-consistency of the data can be seen by scaling the slopes of the other fits by $\ln(\beta^{-1})$ [see (2)]. The *dotted* and *dashed lines* correspond to such a scaling (relative to $A_{1/3}$) of $A_{1/2}$ and $A_{2/3}$, respectively

the background variation, analysis of the data was done for both largest- and smallest-possible background levels, and uncertainties assigned accordingly.

After the background was determined and subtracted, the peak intensity was found and three numbers were computed: $A_{1/3}$, $A_{1/2}$ and $A_{2/3}$. These numbers corresponded to the areas throughout which the intensity of the molasses exceeded 1/3, 1/2, and 2/3, respectively, of the peak intensity.

If one considers a three-dimensional Gaussian distribution of atoms, expanding in a spherically-symmetric cloud, with an e^{-1} radius at a time $t = 0$ of $(4D_x t_0)^{1/2}$, the density of atoms, ρ, is then given by

$$\rho(x,y,z,t) = \exp(-t/\tau)N_0[4\pi D_x(t+t_0)]^{-3/2} \times \exp\left(\frac{-(x^2+y^2+z^2)}{4D_x(t+t_0)}\right). \quad (1)$$

Here, D_x is the spatial-diffusion constant, N_0 is the number of atoms in the cloud at $t = 0$, and τ is some characteristic lifetime of atoms in the trap due to, for example, background collisions. The camera integrates over the z-axis, and the area A_β defined by the radius at which the intensity of the image falls to β of its peak value, is given by

$$A_\beta = 4\pi t D_x \ln(\beta^{-1}). \quad (2)$$

This analysis assumes that any loss mechanism is independent of density. This may not be true at very high densities where collisions between cold atoms could occur. In our experiment, however, all measurements started several hundred milliseconds after the MOT was released; consequently, the densities had fallen to levels where trap loss from collisions between atoms in the expanding cloud was negligible. Our data supported this assumption, as the expansion of the area A_β was always very linear at the beginning of the movies (just after the MOT was released).

An example of data taken from a single movie is shown in Fig. 1. This movie was taken with a normalized intensity of $I/I_0 = 1.05$ for each of the six laser beams with a detuning of 4.75 Γ. I_0 is the saturation intensity of a transition having a Clebsch–Gordon coefficient of 1, and is defined below in (9); for rubidium, $I_0 = 1.62\,\mathrm{mW/cm^2}$. The atoms diffuse with A_p increasing linearly until they begin to reach the edge of the molasses beams. When they hit an edge, the area either remained constant or decreased due to loss of signal (as is the case in Fig. 1). Analysis of the data proceeded until the cloud visually reached an edge, or the signal-to-noise ratio became too small. Additionally, the first few frames of each movie were eliminated as they contained pixels affected by saturation from the high initial intensity of the trap.

For each of the movies, a linear least-squares fit was applied to data which were obtained before the atoms diffused to the edge of the molasses region (Fig. 2). A diffusion constant was calculated for each A_β using (2). A weighted average of the three values (one for each area, $A_{1/3}$, $A_{1/2}$, and $A_{2/3}$) was computed with weights determined by the goodness of their linear fits. Values for D_x obtained for the different values of β typically agree to within 8%. These values are plotted as a function of intensity for several detunings for the lin $\perp$ lin data in Fig. 3.

Similar, but less extensive, measurements were taken after a significant optical realignment. These data are not presented in this paper (intensities and detunings do not match exactly, so a direct comparison is not possible), however, the values of the spatial diffusion lie within $\approx$10% of the values given here. This confirms our confidence in the data presented here.

In this experiment our efforts were focused primarily on measurements of lin$\perp$lin data. We did, however, take data for a few conditions using $\sigma^+ - \sigma^-$ molasses. The diffusion constants were approximately a factor of 2 higher than those measured in the lin $\perp$ lin configuration with similar detunings and intensities.

Uncertainties for the data of Fig. 3 were evaluated in two ways; the statistical uncertainty of the fits added in a weighted sum, or the difference in values computed when

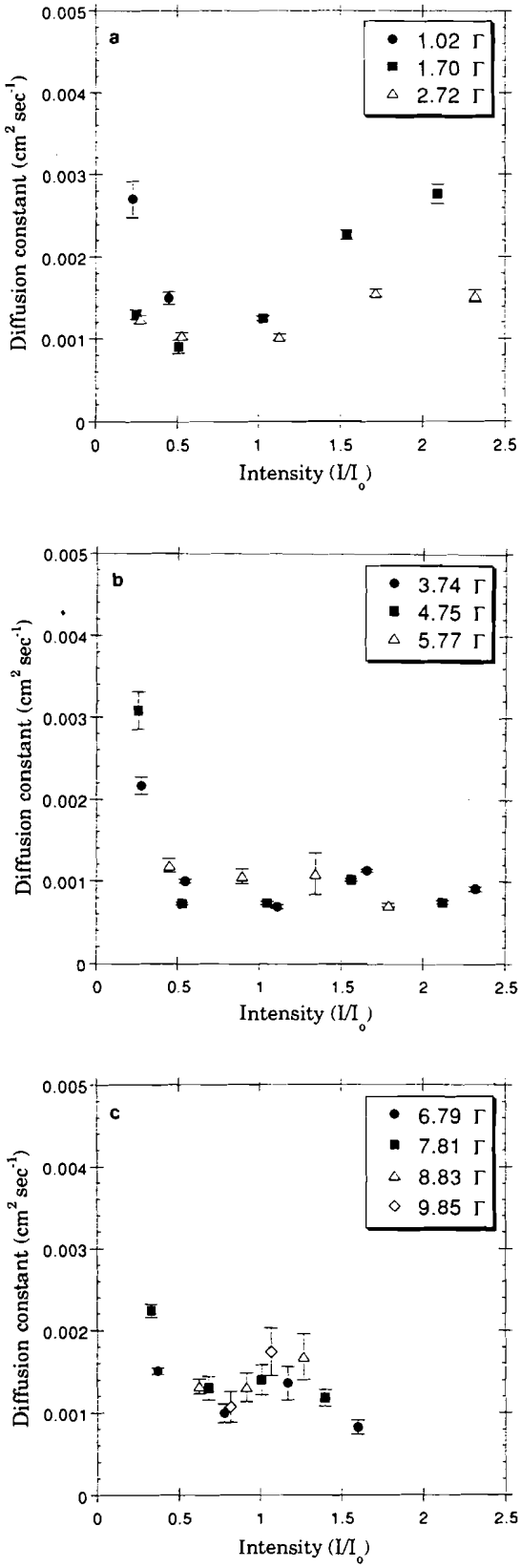

Fig. 3a–c. Lin ⊥ lin data for a variety of detunings as a function of intensity I/I_0. Detunings vary between -1.02Γ and -9.85Γ. Uncertainties, as discussed in Sect. 1.3, are indicated for all points

using the range of possible backgrounds. In ≈ 60% of the movies, the uncertainty due to background subtraction was greater than the statistical spread. The error bars shown on the graphs in Fig. 3 correspond to the larger of the two contributions. In each case, error bars were significantly smaller than the magnitude of the observed value.

We note that the smallest measured value of the diffusion coefficient was $\approx 6\times10^{-4}\,\mathrm{cm^2\,s^{-1}}$. For a 1 cm molasses and this value of the diffusion coefficient, equation (30) of [3] implies a molasses lifetime of approximately 40 s. We were not able to observe lifetimes of this length due, presumably, to background-gas collisions. The longest lifetime we observed was 13 s for a 1.8 cm diameter molasses. This is reasonable given the background pressure of 10^{-7} Pa.

2 Theoretical approach to the spatial diffusion in optical molasses

We present in this section a few theoretical considerations about the problem of spatial diffusion of atoms in optical molasses. Let us emphasize that we will not give here a complete solution to this problem, which remains one of the difficult points in an understanding of laser cooling. What we will try to do here is to start with the standard well-known results for Brownian motion, and to increase gradually the complexity of our model to arrive at a description which models, in a qualitatively satisfactory way, the experimental results presented above.

We first consider sub-Doppler cooling and more specifically the Sisyphus mechanism in which cooling occurs because of correlations between light shifts of Zeeman ground states and the optical pumping rates between these states. The analytical results derived below hold for the cooling of an atom with a $J_g = 1/2 \leftrightarrow J_e = 3/2$ transition, in a 1D molasses formed by a pair of counter-propagating waves with orthogonal linear polarizations (lin ⊥ lin configuration).

2.1 Spatial diffusion in standard Brownian motion

The random motion of a large Brownian particle with a mass M in a bath of small molecules is well described in terms of two components: a linear friction force $f(v) = -\alpha v$, where α is a constant, indicating how the average velocity of the Brownian particle is damped in the bath; and a constant momentum-diffusion coefficient D_p giving the heating of the Brownian particle due to the randomness of collisions of bath molecules.

The time evolution of the average square momentum of a Brownian particle is given by

$$\frac{\mathrm{d}\langle p^2\rangle}{\mathrm{d}t} = -\frac{2\alpha}{M}\langle p^2\rangle + 2D_p\,. \tag{3}$$

The fluctuation-dissipation relation relates D_p, α, and the temperature T of the bath as $D_p = Mk_BT\alpha$, where k_B is Boltzmann's constant. It ensures that, in a time $\tau_v = M/\alpha$, the Brownian particle reaches a steady-state corresponding to a thermal equilibrium with the bath such that

$$M\bar{v}^2 = \frac{D_p}{\alpha} = k_BT\,. \tag{4}$$

On a time scale long compared to τ_v, as shown for instance in the Appendix of this paper, the motion of the particle is diffusive, i.e., the average of the square of the position of the Brownian particle increases linearly with time:

$$\frac{d\langle x^2\rangle}{dt} = 2D_x \tag{5}$$

The spatial diffusion D_x is given by

$$D_x = \frac{D_p}{\alpha^2} = \bar{v}^2\tau_v\,. \tag{6}$$

This expression has the standard form for a diffusion constant, i.e., the product of the square of the random-walk step size $\bar{v}\tau_v$, times the rate of random steps $1/\tau_v$.

2.2 *Spatial diffusion for molasses in the linear regime*

The simplest mechanism for laser cooling, Doppler cooling, is well described by the previous linear approach. The behavior of the spatial-diffusion coefficient for Doppler cooling has been discussed in detail in [3], so that we just briefly review it here. The friction coefficient and the momentum-diffusion coefficient along a given axis are given by [3]

$$\alpha = \hbar k^2 \frac{8|\delta|\Gamma}{4\delta^2+\Gamma^2} s_0\,, \tag{7}$$

$$D_p = \hbar^2 k^2 \Gamma s_0\,, \tag{8}$$

where Γ is the natural decay rate of the population of the excited state of the cooling transition, $k = 2\pi/\lambda$ is the wave number, and $\delta = \omega_L - \omega_A$ is the detuning between laser and atomic frequencies. The saturation parameter is related to the Rabi frequency Ω associated with each traveling wave forming the 1D molasses by

$$s_0 = \frac{2\Omega^2}{4\delta^2+\Gamma^2}\,, \quad \text{with} \quad \frac{\Omega^2}{\Gamma^2} = \frac{I}{2I_0}\,. \tag{9}$$

I is the intensity in each traveling wave forming the molasses and I_0 is the saturation intensity. We assume $s_0 \ll 1$ throughout this section, which is well satisfied for the experimental conditions. We recall that Doppler cooling, described by the friction coefficient α, originates from imbalance between radiation-pressure forces exerted by the Doppler-shifted waves forming the molasses. The momentum-diffusion coefficient D_p is related to the fluctuations of the number of photons absorbed in each wave forming the molasses, and to the fluctuations of momentum carried away by the fluorescence photons. For detunings δ such that $|\delta| > \Gamma$, the spatial-diffusion coefficient deduced from (6–8) is

$$D_x = \frac{\Gamma}{k^2}\left(\frac{\delta}{\Gamma}\right)^4 \frac{I_0}{I}\,. \tag{10}$$

It is well known that Doppler-cooling theory cannot account for the ultra-low temperatures observed in the molasses. When comparing the prediction (10) to the experimental results sketched in Fig. 3, it clearly appears that Doppler-cooling theory cannot explain either the observed magnitude of the spatial-diffusion coefficient, or its dependence on laser parameters. For instance, for $I = I_0$, the increase of D_x as $(\delta/\Gamma)^4$ is not observed at all, since D_x varies by less than a factor 2 when $|\delta|/\Gamma$ goes from 1.70 to 9.85. Also, the values for D_α derived from (10) are much larger than the experimental results. For example, taking again $I = I_0$ and $|\delta|/\Gamma = 4.75$, we get $D_x \approx 3\,\mathrm{cm^2/s}$ which is more than 1000 times larger than the experimental value.

In order to explain the ultra-low temperatures observed in the molasses, one has to refer to polarization-gradient cooling. We now consider this type of cooling mechanism, and we focus specifically on Sisyphus cooling. In some particular conditions, obtained for relatively large laser intensities and small detunings, the linear Brownian motion approach (i.e., the frictional force is linear in momentum and the diffusion coefficient is independent of v) can be used for describing the Sisyphus mechanism. In a lin $\perp$ lin 1D model for a $J_g = 1/2 \leftrightarrow J_e = 3/2$ transition [5], the friction coefficient α and the momentum-diffusion coefficient D_p are given by

$$\alpha = 3\hbar k^2 \frac{|\delta|}{\Gamma}\,, \tag{11}$$

$$D_p = D_{p1} + D_{p2}\,, \tag{12}$$

with

$$D_{p1} \cong \hbar^2 k^2 s_0 \Gamma\,, \tag{13}$$

$$D_{p2} = \frac{3}{4}\hbar^2 k^2 s_0 \frac{\delta^2}{\Gamma}\,. \tag{14}$$

There are now two contributions to the momentum-diffusion coefficient. The first is identical to the one found in the Doppler-cooling model, assuming that all the fluorescence photons are emitted along the cooling axis ("true 1D model"). The second contribution originates from the fluctuations of the light shift-induced force, as the atom randomly jumps from one Zeeman ground state to another.

For detunings $|\delta| > \Gamma$, the contribution of D_{p2} dominates and this model leads to an equilibrium "temperature" for the molasses given by

$$M\bar{v}^2 = k_B T = \frac{D_p}{\alpha} \cong \frac{1}{4}\hbar|\delta| s_0\,. \tag{15}$$

Replacing the values of α and D_p in (6), we obtain

$$D : D_x = \frac{1}{48}\frac{\Gamma}{k^2}\left(\frac{\Gamma}{\delta}\right)\frac{I}{I_0}\,. \tag{16}$$

This prediction, based on a linear Brownian-motion approach, is valid when the average displacement of an atom during an optical pumping time τ_p is small compared to the reduced laser wavelength $\lambda/2\pi$ [5]. The validity condition for (16) is therefore

$$k\bar{v}\tau_p \ll 1\,. \tag{17}$$

The optical pumping time is $\tau_p = 9/(2\Gamma s_0)$. Substituting (15) into (17), we obtain

$$D : \left(\frac{|\delta|}{\Gamma}\right)^{3/2} \ll 6\left(\frac{I}{I_0}\right)^{1/2}\,, \tag{18}$$

where the numeric coefficient was obtained using parameters for rubidium's mass, linewidth and wavelength.

To extend this model to 3D, we need to know how the various cooling parameters τ_p, α, and D_p are changed. For τ_p we can use the simple argument that if the intensity I in each wave remains the same, the total intensity incident on

an atom is multiplied by 3, so that τ_p is divided by 3. For α and D_p this kind of scaling is more difficult, so that we turn to a numerical calculation of these coefficients. We consider again an atom with a $J_g = 1/2 \leftrightarrow J_e = 3/2$ transition, moving now in the field of 3 standing waves, each in the lin $\perp$ lin configuration [11]. One finds that in the range of parameters of interest here, α is divided by 7 while D_p is divided by 3, so that the temperature is increased by a factor 2.3. Using this result in (6), we are led to a multiplication factor for D_x of $7 \times 7/3 \approx 16$ so that we get

$$\text{3D}: \quad D_x \cong \frac{1}{3}\frac{\Gamma}{k^2}\left(\frac{\Gamma}{\delta}\right)^2 \frac{I}{I_0}. \tag{19}$$

The validity condition (18) is also modified, it becomes

$$\text{3D}: \quad \left(\frac{|\delta|}{\Gamma}\right)^{3/2} \ll 12\left(\frac{I}{I_0}\right)^{1/2}. \tag{20}$$

Experimental results obtained in 3D included a range of I/I_0 between 0.3 and 2. Detunings satisfying (20) should then be much smaller than 5Γ. Therefore, only the first two detunings, -1.02 and -1.7Γ, are in the validity range for this approximation. Although there are insufficient data at $\delta = -1.02\Gamma$ for a comparison, one finds that at -1.7Γ (Fig. 3a), D_x varies linearly with intensity for $I/I_0 > 0.5$. The order of magnitude given by (19) is also satisfying considering the difference between our model atomic transition and the real one; for $I = I_0$ and $\delta = -1.7\Gamma$ we obtain $\approx 7 \times 10^{-4}\,\text{cm}^2\,\text{s}^{-1}$, which is within a factor 2 of the experimental result.

2.3 Beyond the linear regime

As we have seen, most of the experimental points are outside of the range of validity given by (18) and (20) of the linear treatment of molasses. To study one-dimensional situations beyond this, a simple extension of the Brownian-motion model has been proposed in [12]. It consists in taking

$$f(v) = \frac{-\alpha v}{1 + (v/v_c)^2}, \tag{21}$$

$$D_p(v) = D_{p1} + \frac{D_{p2}}{1 + (v/v_c)^2}, \tag{22}$$

where the velocity v_c is such that $2kv_c\tau_p = 1$. (For simplicity we have dropped a few unessential terms which appear in [12], so that some minor differences appear between our results and those of Castin et al. This has no consequence on the principal conclusions of the model.) For velocities $|v| \ll v_c$ which correspond to (17), we recover the previous linear model. For $|v| \gg v_c$, which corresponds to the case where the atom travels over several wavelengths between two optical pumping processes, the force and the part of the diffusion coefficient due to fluctuations of the dipole force are reduced. This model leads to a steady-state momentum distribution $\pi(v)$ given in [12] (see also the Appendix of this paper):

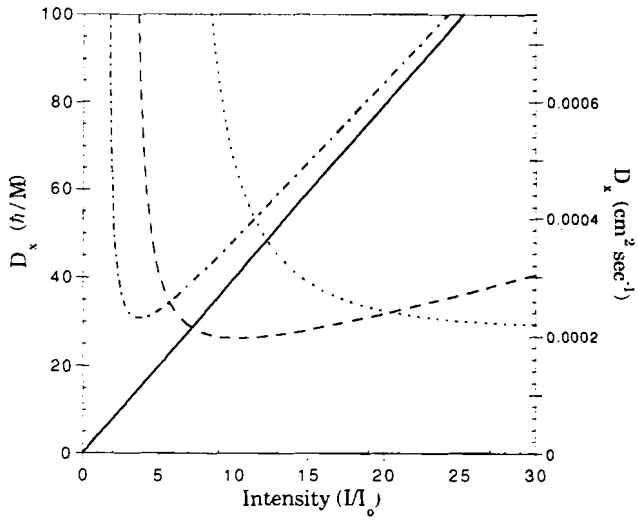

Fig. 4. The theoretical spatial-diffusion coefficient D_x, for a 1D model, presented in units of $\hbar/M$ ($\hbar/M = 7.5 \times 10^{-6}\,\text{cm}^2/\text{s}$ for ^{85}Rb), as a function of intensity I/I_0 for three values of detuning $\delta = -2\Gamma$ (*dashed-dotted line*), -4Γ (*dashed line*), and -8Γ (*dotted line*). These curves were obtained using (A20), which takes into account velocity dependence of the force and the momentum-diffusion coefficient given in (21) and (22). The *solid line* is the prediction of the linear model (16). It is indicated only for a detuning of $\delta = -2\Gamma$. These curves were plotted for $M\Gamma/\hbar k^2 = 760$, corresponding to rubidium's atomic parameters. Although a direct comparison with the (3D) experimental values is not appropriate, we have included, on the right-hand side, an additional scale to allow magnitude comparisons

$$\pi(v) = \frac{\pi(0)}{\left[1 + (v/\bar{v}_c)^2\right]^A}, \tag{23}$$

with

$$\bar{v_c} = \frac{\sqrt{3}}{2} v_c \frac{|\delta|}{\Gamma}, \tag{24}$$

$$A = \frac{1}{108}\frac{\hbar|\delta|s_0}{E_R}. \tag{25}$$

The parameter A is proportional to the typical light shift $\hbar\delta s_0$ measured in units of recoil energy $E_R = \hbar k^2/2M$.

This steady-state distribution nicely reproduces the observed disintegration (also known as *décrochage*) of the molasses when the light shift is too small. In our model, the disintegration corresponds to the situation $A < 1/2$, for which one can no longer normalize the distribution $\pi(v)$. By contrast, for large A, one can show that one recovers a Maxwellian velocity distribution with $M\bar{v}^2 = \hbar\delta s_0/4$.

Using the standard theory of adiabatic elimination of a fast variable (momentum) with respect to a slow one (position), one can now deduce from (21) and (22) an equation for $\langle x^2 \rangle$ similar to (5). The general expression for the spatial coefficient D_x is given in the Appendix (A20). In Fig. 4, we have plotted the variations of D_x with the laser intensity I for three different detunings, $|\delta|/\Gamma = 2$, 4, and 8.

For the smallest detuning $|\delta|/\Gamma = 2$, two regimes clearly appear. At high intensities, D_x varies linearly with I and we recover the prediction given in (16). When the intensity decreases, D_x goes through a minimum and then increases to infinity. The same type of variations could be found for

the two other detunings appearing in Fig. 4, but the linear regime occurs at much higher intensities [as expected from (18)], and it is not represented in Fig. 4. We do, however, observe the divergence of D_x at low intensity for each detuning. From the expression of D_x given in (A20), we see that the divergence occurs for a constant value of the light-shift corresponding to a value for the parameter A equal to 2.5. Below this value, the motion becomes non-diffusive and $\langle x^2(t)\rangle$ increases faster than t. We note that this requirement for diffusive motion is 5 times more constraining in terms of laser intensity than the condition for having a normalizable steady-state velocity distribution. We therefore expect that even for molasses perfectly "well behaved" in terms of momentum distribution, the spatial motion may present deviations from the diffusive law. This may explain why it is so difficult to observe the disintegration of the velocity distribution in experiments with optical molasses: the divergence of the spatial diffusion destroys the molasses before the velocity distribution disintegrates.

The minimal value of D_x as a function of intensity is nearly the same for the three curves of Fig. 4. The absolute minimum of D_x, found for $|\delta|/\Gamma = 4.3$ and $A = 9.5$, is

$$(D_x)_{\min} \cong 26\frac{\hbar}{M}. \tag{26}$$

When used with rubidium's parameters for mass, linewidth and wavelength, these values of A and δ correspond to a saturation parameter $s_0 = 0.17$, and a minimum spatial-diffusion coefficient of $0.2 \times 10^{-3}\,\mathrm{cm^2/s}$. It is remarkable that the absolute minimum value for D_x, derived from such a simple 1D theory, is quite close to the minimum 3D experimental value of $0.6 \times 10^{-3}\,\mathrm{cm^2/s}$.

In order to improve the agreement between the theoretical predictions and the experimental results, one would need to perform a real 3D treatment. One should also consider an atomic transition more realistic than the $J_g = 1/2 \leftrightarrow J_e = 3/2$ scheme. Such a treatment would lead to new values for the main parameters of Fig. 4, which are: (i) the slope of the linear part in the variations of D_x with I/I_0, (ii) the light shift below which D_x diverges, and (iii) the value of the absolute minimum of D_x. The modification of the slope of the linear part of the variation of D_x vs. I/I_0 for a simple approximation of the 3D case has already been given in (19). We have seen that it reproduces the experimental results within a factor 2.

2.4 *Extension of theoretical models to three dimensions*

In order to determine the experimental value of the light shift below which D_x diverges, we have replotted in Fig. 5 the experimental points as a function of the typical light shift $\hbar|\delta|s_0$ in units of $\hbar\Gamma$. The low light-shift part of the curve suggests a divergence near $\hbar|\delta|s_0 \cong 0.01\hbar\Gamma$, which corresponds to $\hbar|\delta|s_0 = 15E_R$. This value of the light shift in units of E_R corresponds, within a factor of 2, to the values for which disintegration was observed in previous measurements [7, 9]. This value of the light shift is, however, 20 times lower than the 1D prediction. It is difficult to give an account for such a large factor in absence of a real 3D treatment of spatial diffusion in optical molasses. Nevertheless, we can compare

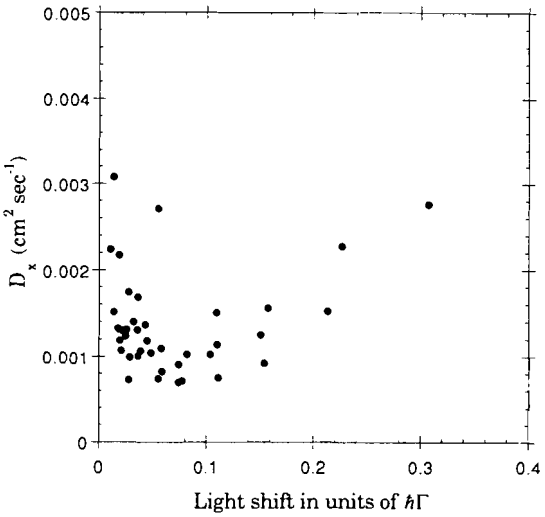

Fig. 5. Diffusion constants for all data as a function of light shift ($\hbar|\delta|s_0$) in units of $\hbar\Gamma$. For low values of the light shift, the diffusion coefficient increases, with an apparent divergence located approximately at $\hbar|\delta|s_0 \cong 0.01\hbar\Gamma$

results obtained in 1D and in 2D for such threshold light shifts, and assume that the tendency from 1D to 2D will not reverse from 2D to 3D. Consider, for instance, the population of the quantum ground state of atomic motion in the light shift potential. In 1D, for the laser configuration studied above, this population was maximal for $\hbar|\delta|s_0 = 90E_R$ [13]. In 2D, for the laser configuration formed by two standing waves aligned along two orthogonal axes x and y and with linear polarizations y and x, the position of the maximum is notably reduced to $\hbar|\delta|s_0 = 22E_R$ [14]. We can expect that a reduction of a similar order of magnitude would be found for the spatial-diffusion coefficient; however, this has not yet been checked.

The 3D calculation of the minimum value of the spatial-diffusion coefficient is also an open problem. It cannot be derived simply from an extrapolation of 1D results, because there is a qualitative change in the nature of the problem with the change of dimensionality. In 1D, between two spontaneous emissions, the atom travels on a straight line with a constant mechanical energy. In 2D or 3D, the trajectory of the atom between two spontaneous emissions is very complicated because the atom is deflected by potential hills created by the light. These hills are regularly spaced with a spatial period equal to a fraction of an optical wavelength λ. Depending on the nature of this Hamiltonian motion (chaotic or regular), this may or may not lead to a different type of spatial diffusion with a mean free path, or decorrelation length, of a few spatial periods of the potential. In the case where the motion is diffusive, if we neglect the effect of spontaneous emission, and if we take $n\lambda$ to be the decorrelation length, where n is a numerical factor, we obtain for the spatial-diffusion coefficient

$$D_x \cong (n\lambda)^2\left(\frac{\bar{v}}{n\lambda}\right) = n\lambda\bar{v} = 2\pi n\left(\frac{\hbar}{M}\right)\left(\frac{\bar{v}}{\hbar k/M}\right). \tag{27}$$

For a given detuning this formula should hold in the intermediate regime where the intensity is above the disintegration-threshold intensity, but where it remains below the intensity

corresponding to the linear regime studied in Sect. 2.2 (20). In the linear regime, the atom randomly jumps several times between various Zeeman ground-state sublevels when traveling over a single wavelength; consequently, scattering by potential hills corresponding to a given sublevel is effectively averaged out. Let us assume a velocity $\bar{v}$ of 6 recoil velocities $\hbar k/M$ (which is typical for our intensities and detunings). From (27), we find that for minimum diffusion coefficients of the order of $0.6 \times 10^{-3}\,\mathrm{cm^2/s}$ (i.e., $80\hbar/M$) we get a decorrelation length of approximately 2λ. A 2D and a 3D Monte-Carlo analysis of the classical motion of the atom in the light shift potential is currently underway to investigate this problem in more detail.

3 Conclusion

We have measured spatial diffusion parameters for the lin $\perp$ lin configuration of a 3D optical molasses, as well as some values for the $\sigma^+ - \sigma^-$ configuration. Diffusion constants inferred from previous measurements of the lifetime of a sodium molasses [1, 3] are at least two orders of magnitude larger than the minimum diffusion constant measured in this work. We have also presented a 1D (lin $\perp$ lin) model for spatial diffusion in optical molasses, with a force varying nonlinearly with velocity, and with a velocity-dependent diffusion coefficient. We have also made a few comments on possible extensions of our predictions to the 3D problem. The predictions of the model agree reasonably well with the experimental results and qualitatively reproduce their behavior. Specifically, this includes the existence of a minimum light shift for which diffusive motion can be observed, and above this light shift, an increase of D_x with I/I_0 if the detuning is small, or a plateau value for D_x if the detuning is large. The theory also predicts a minimum spatial-diffusion coefficient ($0.2 \times 10^{-3}\,\mathrm{cm^2/s}$ for Rb) which is within a factor of 3 of the measured value.

Two different natural scales appear for the diffusion constant. The first one is Γ/k^2 ($5.7 \times 10^{-3}\,\mathrm{cm^2/s}$ for Rb). It shows up both for the Doppler-cooling model, and in the linear treatment of Sisyphus cooling. This scale, Γ/k^2, appears multiplied by functions of intensity or detuning that can be arbitrarily large or small, provided the validity condition of the linear model is fulfilled. The second scale is $\hbar/M$ ($7.5 \times 10^{-6}\,\mathrm{cm^2/s}$ for Rb). It appears in the determination of the absolute minimum of D_x, with a multiplicative factor depending on the dimensionality. The existence of these two scales is related to two scales which appear in the determination of the temperature: (1) $\hbar\Gamma$ for Doppler or Sisyphus cooling in the linear regime (again with a multiplicative factor depending on I/I_0 and δ/Γ), and (2) the recoil energy $E_R = \hbar^2k^2/2M$ which gives the scale of the minimum temperature achievable with polarization-gradient cooling. Therefore, it would be quite interesting to test the prediction that the scale $\hbar/M$ appears as an absolute limit for D_x, by determining experimentally the minimum value of the spatial-diffusion coefficient for atoms of various masses.

Acknowledgements. C.G. thanks the Alexander-von-Humboldt foundation, and T. W. H. the Joyce foundation and the Research Corporation for their financial support. J. D. thanks the NIST group for their hospitality during the period in which a portion of this work was completed, and he is indebted to Yvan Castin for many stimulating discussions. He also acknowledges partial financial support from DRET and NIST. This work was partially supported by the U.S. Office of Naval Research.

Appendix

The purpose of this Appendix is to present the general derivation of a spatial-diffusion coefficient for the 1D problem of an atom moving in molasses. We assume that the atomic equation of motion has the standard form of a Fokker–Planck–Kramers equation [15]. The atomic phase-space distribution $W(x,v,t)$ evolves then as

$$\frac{\partial W}{\partial t} + v\frac{\partial W}{\partial x} = \frac{\partial}{\partial v}\left(-\frac{F(v)}{M}W + \frac{D_p(v)}{M^2}\frac{\partial W}{\partial v}\right). \tag{A1}$$

We suppose that the force $F(v)$ and the momentum-diffusion coefficient $D_p(v)$ are known, and we want to derive an equation of motion for the position distribution $\rho(x,t)$

$$\rho(x,t) = \int \mathrm{d}v W(x,v,t). \tag{A2}$$

Since the force $F(r)$ and the momentum-diffusion coefficient $D_p(v)$ depend only on the velocity v and not on the position x, the problem is invariant under any space translation and we may hope to be able to derive a diffusion equation for $\rho(x,t)$. Actually, we will see that this is indeed possible provided that $F(v)$ and $D_p(v)$ "behave correctly" when v goes to infinity.

We follow the standard procedure of the adiabatic elimination of a fast variable (here, the velocity v) to keep only the evolution of a slow variable (here, the position x) [15,16]. The equation of motion (A1) can be written formally

$$\frac{\partial W}{\partial t} = \left(L^{(0)} + \varepsilon L^{(1)}\right) \bullet W, \tag{A3}$$

where

$$L^{(0)} \bullet W = \frac{\partial}{\partial v}\left(-\frac{F(v)}{M}W + \frac{D_p(v)}{M^2}\frac{\partial W}{\partial v}\right), \tag{A4}$$

$$\varepsilon L^{(1)} \bullet W = -v\frac{\partial W}{\partial x}. \tag{A5}$$

$L^{(0)}$ and $L^{(1)}$ are linear operators on W, acting, respectively, in velocity space and position space, and ε is an expansion parameter. The principle of adiabatic elimination is that the velocity part of W nearly reaches a steady state such that $L^{(0)} \bullet W = 0$. One is then left only with the evolution of the position part of W, which leads to the required spatial-diffusion coefficient.

We introduce the normalized function $\pi(v)$ such that $L^{(0)} \bullet \pi(v) = 0$:

$$\pi(v) = \pi(0)\exp\left(\int_0^v \frac{MF(v')}{D_p(v')}\mathrm{d}v'\right), \tag{A6}$$

$$1 = \int_{-\infty}^{+\infty} \pi(v)\mathrm{d}v, \tag{A7}$$

and we write

$$W(x,v,t) = \rho(x,t)\pi(v) + \delta W(x,v,t). \tag{A8}$$

The quantity δW is a small correction to the adiabatic solution $\rho(x,t)\pi(v)$, and it is defined such that

$$\int_{-\infty}^{+\infty} \delta W(x,v,t)\mathrm{d}v = 0\,. \tag{A9}$$

We now insert (A8) into the equation of motion (A1) or (A3), and we integrate over v. Since $\pi(v)$ is an even function of v, we get

$$\frac{\partial \rho(x,t)}{\partial t} = \int_{-\infty}^{+\infty} \varepsilon L^{(1)} \bullet \delta W(x,v,t)\mathrm{d}v\,. \tag{A10}$$

We now need δW at the lowest order in ε. The equation of motion for δW, also deduced from (A1) or (A3), is

$$\frac{\partial}{\partial t}(\delta W) = L^{(0)} \bullet (\delta W) + \varepsilon L^{(1)} \bullet (\rho\pi)\,, \tag{A11}$$

where terms in $\varepsilon L^{(1)} \bullet (\delta W)$ have been neglected. To first order in ε, the solution of (A11) is such that

$$L^{(0)} \bullet (\delta W) = -\varepsilon L^{(1)} \bullet (\rho\pi)\,. \tag{A12}$$

We now use the explicit form (A4) of the operator $L^{(0)}$ to invert this relation and obtain δW. After simple algebra, we get

$$\delta W(x,v,t) = M^2\pi(v)\frac{\partial \rho(x,t)}{\partial x}\int_0^v \frac{\phi(v')}{D_p(v')\pi(v')}\mathrm{d}v'\,, \tag{A13}$$

where we have introduced the function

$$\phi(v') = \int_{v'}^{+\infty} v''\pi(v'')\mathrm{d}v''\,. \tag{A14}$$

Finally, inserting the expression (A13) for δW into the equation of evolution (A10) for $\rho(x,t)$ we obtain a closed equation for ρ which has the form of a diffusion equation:

$$\frac{\partial \rho(x,t)}{\partial t} = D_x\frac{\partial^2 \rho(x,t)}{\partial x^2}\,, \tag{A15}$$

with

$$\begin{aligned} D_x &= M^2\int_{-\infty}^{+\infty} v\pi(v)\left(\int_0^v \frac{\phi(v')}{D_p(v')\pi(v')}\mathrm{d}v'\right)\mathrm{d}v\,, \\ &= M^2\int_{-\infty}^{+\infty} \frac{\phi(v)^2}{D_p(v)\pi(v)}\mathrm{d}v\,. \end{aligned} \tag{A16}$$

A.1 Examples

A.1.1 Linear case. We have for a linear force and a constant momentum-diffusion coefficient,

$$\pi(v) = \frac{1}{\bar{v}\sqrt{2\pi}}\exp\left(-v^2/2\bar{v}^2\right)\,, \tag{A17}$$

with $\bar{v} = \sqrt{D_p/\alpha M}$. We then calculate the function $\phi(v)$ and find

$$\phi(v) = \frac{\bar{v}}{\sqrt{2\pi}}\exp\left(-v^2/2\bar{v}^2\right)\,, \tag{A18}$$

from which we deduce

$$D_x = \frac{D_p}{\alpha^2}\,. \tag{A19}$$

A.1.2 Sisyphus cooling. Using (21) and (22) for the friction and the diffusion coefficient, we first derive from (A16) the expression (23) for $\pi(v)$. Then, a lengthy but straightforward calculation starting from (A15) leads to

$$\begin{aligned} D_x = \frac{9}{2}\frac{\hbar}{M}&\frac{A^3}{(A-1)(A-3/2)(A-5/2)} \\ &\times\left(A-\frac{5}{2}+\frac{3\delta^2}{8\Gamma^2}\right)\frac{\Gamma}{|\delta|}\,. \end{aligned} \tag{A20}$$

The three curves of Fig. 4 have been drawn from this analytical expression for D_x. The divergence of D_x which appears in (A20) for $A < 5/2$ can be understood simply. D_x is defined only if the integral over v entering in (A16) converges as v goes to $\pm\infty$. Since $\pi(v)$ varies as v^{-2A} at infinity, $\phi(v)$ varies as v^{2-2A}; the diffusion coefficient $D_{p(v)}$ tends to a constant value D_{p1}, so that the integral of (A16) converges if $4-2A < -1$, or $A > 5/2$.

References

1. S. Chu, L. Hollberg, J. Bjorkholm, A. Cable, A. Ashkin: Phys. Rev. Lett. **55**, 48 (1985)
2. W. Phillips, J. Prodan, H. Metcalf: J. Opt. Soc. Am. B **2**, 1751 (1985)
3. P.D. Lett, W.D. Phillips, S.L. Rolston, C.E. Tanner, R.N. Watts, C.I. Westbrook: J. Opt. Soc. Am. B **6**, 2084 (1989)
4. P. Lett, R. Watts, C. Westbrook, W. Phillips, P. Gould, H. Metcalf: Phys. Rev. Lett. **61**, 169 (1988)
5. J. Dalibard, C. Cohen-Tannoudji: J. Opt. Soc. Am. B **6**, 2023 (1989)
6. P.J. Ungar, D.S. Weiss, E. Riis, S. Chu: J. Opt. Soc. Am. B **6**, 2058 (1989)
7. C. Salomon, J. Dalibard, W.D. Phillips, A. Clairon, S. Guellati: Europhys. Lett. **12**, 683 (1990)
8. E.L. Raab, M. Prentiss, A. Cable, S. Chu, D.E. Pritchard: Phys. Rev. Lett. **59**, 2631 (1987)
9. C. Gerz, T.W. Hodapp, P. Jessen, K.M. Jones, W.D. Phillips, C.I. Westbrook, K. Mølmer: Europhys. Lett. **21**, 661 (1993)
10. J.V. Prodan, W.D. Phillips: Prog. Quant. Electr. **8**, 231 (1984)
11. K. Mølmer: Phys. Rev. A **44**, 5820 (1991), and private communication
12. Y. Castin, J. Dalibard, C. Cohen-Tannoudji: In *Light Induced Kinetic Effects on Atoms, Ions and Molecules*, ed. by L. Moi, S. Gozzini, C. Gabbanini, E. Arimondo, F. Strumia (ETD Editrice, Pisa 1991)
13. Y. Castin, J. Dalibard: Europhys. Lett. **14**, 761 (1991)
14. K. Berg-Sørensen, Y. Castin, K. Mølmer, J. Dalibard: Europhys. Lett. **22**, 663 (1993)
15. N.G. van Kampen: *Stochastic Processes in Physics and Chemistry* (North-Holland, Amsterdam 1981), Chap. 8
16. N.G. van Kampen: Phys. Rep. **124**, 69 (1985)